

Chaperone-like *N*-Methyl Peptide Inhibitors of Polyglutamine Aggregation[†]

Jennifer D. Lanning,[‡] Andrew J. Hawk,[‡] JohnMark Derryberry,[‡] and Stephen C. Meredith^{*,‡,§}

[‡]Department of Pathology and [§]Department of Biochemistry and Molecular Biology, The University of Chicago, Chicago, Illinois 60637

Received April 21, 2010; Revised Manuscript Received June 17, 2010

ABSTRACT: Polyglutamine expansion in the exon 1 domain of huntingtin leads to aggregation into β -sheet-rich insoluble aggregates associated with Huntington's disease. We assessed eight polyglutamine peptides with different permutations of *N*-methylation of backbone and side chain amides as potential inhibitors of polyglutamine aggregation. Surprisingly, the most effective inhibitor, 5QMe₂ [Anth-K-Q-Q(Me₂)-Q-Q(Me₂)-Q-CONH₂, where Anth is *N*-methylantranilic acid and Q(Me₂) is side chain *N*-methyl Q], has only side chain methylations at alternate residues, highlighting the importance of side chain interactions in polyglutamine fibrillogenesis. Above a 1:1 stoichiometric ratio, 5QMe₂ can completely prevent fibrillation of a synthetic aggregating peptide, YAQ₁₂A; it also shows significant inhibition at substoichiometric ratios. Surface plasmon resonance (SPR) measurements show a moderate *K*_d with very fast *k*_{on} and *k*_{off} values. Sedimentation equilibrium analytical ultracentrifugation indicates that 5QMe₂ is predominantly or entirely monomeric at concentrations of ≤ 1 mM and that it forms a 1:1 stoichiometric complex with a fibril-forming target, YAQ₁₂A. 5QMe₂ inhibits not only nucleation of YAQ₁₂A but also fibril extension, as shown by the fact that it also inhibits seeded fibril growth where the nucleation steps are bypassed. 5QMe₂ acts on its targets only when they are in the PPII-like conformation, but not after they undergo a transition to β -sheets. Thus, 5QMe₂ does not disassemble preformed YAQ₁₂A; this contrasts with our previously described, backbone *N*-methylated inhibitors of β -amyloid aggregation [Gordon, D. J., et al. (2001) *Biochemistry* **40**, 8237–8245; Gordon, D. J., et al. (2002) *J. Pept. Res.* **60**, 37–55]. The mode of action of 5QMe₂ is reminiscent of that of chaperones, because it binds and releases its targets very rapidly and maintains them in a nonaggregation-prone, monomeric state, in this case, the polyproline II (PPII)-like conformation, as shown by circular dichroism spectroscopy.

Expanded polyglutamine (polyQ)¹ tracts are responsible for at least nine neurodegenerative diseases, including Huntington's disease (HD). HD occurs when the polyQ domain of exon 1 of huntingtin protein expands beyond a threshold of approximately 35 residues (1), leading to polyQ aggregation (2–4). PolyQ proteins can form β -sheet-rich fibrils (5, 6). In contrast to many other amyloids (7), polyQ domains have polar side chains, and both these and backbone atoms can form hydrogen bonds. Recent X-ray diffraction and solid-state NMR studies of the glutamine- and asparagine-rich yeast prion proteins Sup35p and Rnq1p show parallel in-register β -sheet segments, possibly

separated by non- β -sheet bend structures in longer peptides (8, 9). Prefibrillar oligomers of β -amyloid are micelle-like and show β -sheet character (10). The structure of polyQ oligomers is not known, however; in contrast to oligomers of β -amyloid, the polar nature of polyQ makes it unlikely that they would be micelle-like. Large, prefibrillar "spheroids" of huntingtin also have been observed, and these acquire β -sheet structure as they mature into fibrils (11). We have recently shown that small, soluble oligomers of short polyQ peptides adopt a polyproline II helix-like structure (12, 18), and thus, the conversion to fibrils may require a transition from this structure to β -sheet.

Inhibitors of protein and peptide aggregation are of value both as molecular probes of the aggregation pathway and as potential therapeutic agents (13–15). We have described peptidic inhibitors of β -amyloid, consisting of an aggregation domain in which alternate residues are *N*-methylated on backbone amides. Such inhibitors (e.g., A β 16–20m) both inhibit fibril formation and disassemble preformed fibrils, by disrupting backbone hydrogen bonding (16, 17).

In this paper, we describe what began as a comparison of *N*-methylation patterns in potential inhibitors of polyQ peptide aggregation. These studies, however, soon produced several surprising results, starting with the observation that side chain *N*-methylations alone yield the most effective inhibitors of all the permutations tested on short polyQ peptides. Subsequent experiments highlighted the importance of side chain interactions in polyQ aggregation and showed that the inhibitors act through a

[†]We acknowledge National Institutes of Health (NIH) Medical Scientist Training Program Grant T32 GM07281 (J.D.L.), NIH Cardiovascular Pathophysiology Training Grant HL07237 (J.D.L.), NIH Grant NS042852 (S.C.M.), and the Alzheimer's Association (IIRG-06-27794).

*To whom correspondence should be addressed: Department of Pathology, 5841 S. Maryland Ave., Chicago, IL 60637. Telephone: (773) 702-1267. Fax: (773) 834-5251. E-mail: scmeredi@uchicago.edu.

¹Abbreviations: AIC, Aikake Information Criterion; Anth, *N*-methylantranilic acid; BOP, benzotriazole-1-yl-oxy-tris(dimethylamino)-phosphonium hexafluorophosphate; CD, circular dichroism; DMF, dimethylformamide; ESI, electrospray ionization; FMOC, 9-fluorenylmethoxycarbonyl; Glu(tBu), *N*- α -FMOC-L-glutamic acid γ -*tert*-butyl ester; HATU, 2-(7-aza-1*H*-benzotriazole-1-yl)-1,1,3,3-tetramethyluronium hexafluorophosphate; HD, Huntington's disease; HPLC, high-performance liquid chromatography; MALDI-TOF, matrix-assisted laser desorption time-of-flight; MBHA, 4-methylbenzhydrylamine; PEG, polyethylene glycol; polyP, polyproline; polyQ, polyglutamine; PPII, polyproline type II; SD, standard deviation; SPR, surface plasmon resonance; TFA, trifluoroacetic acid.

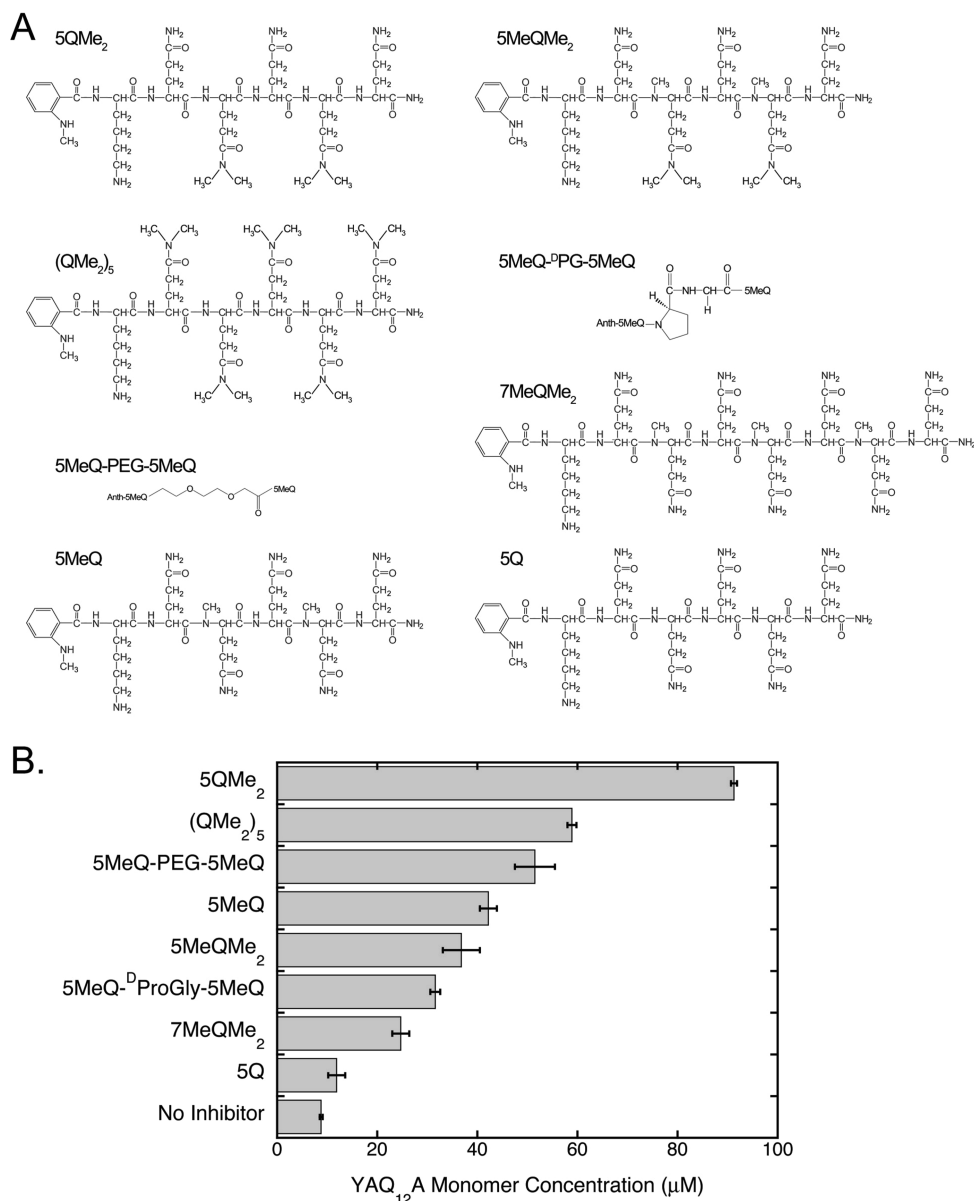


FIGURE 1: Structures of inhibitors tested (A) and results of sedimentation screening assays (B). The peptides represent variations in the pattern of N-methylation. In all cases, the peptides contained an N-terminal *N*-methylanthranilic acid (Anth) and a Lys residue adjacent to the Anth. In the case of 5MeQ-DPG-5MeQ and 5MeQ-PEG-5MeQ, the C-terminal inhibitor domain does not contain a Lys residue. Results are expressed as micromolar concentrations YAQ₁₂A monomer remaining after the incubation. Data are the mean \pm SD of three replicate determinations.

mechanism reminiscent of chaperone proteins. We examined the most effective of these inhibitors in detail and observed that it binds to a target polyQ peptide and inhibits its aggregation by forming a 1:1 stoichiometric complex. It inhibits not only nucleation but also fibril extension, as shown by its ability to inhibit seeded fibril growth in which nucleation steps are bypassed. Furthermore, our data indicate that the effective inhibitors adopt a polyproline II conformation and interact with a polyQ peptide only while it is also in the PPII conformation. These results suggest a scheme for the polyglutamine aggregation pathway more complex than has been appreciated previously.

EXPERIMENTAL PROCEDURES

Peptide Synthesis and Purification. YAQ₁₂A and 5Q were synthesized using standard 9-fluorenylmethoxycarbonyl (Fmoc) chemistry and Rink Amide resin, on an Applied Biosystems model 433A peptide synthesizer. In early experiments, peptides were cleaved from the resin using 9.5 mL of TFA, 0.25 mL of water,

and 0.25 mL of triisopropylsilane. We subsequently observed that both the yields and initial purity of the mixture from the resin were significantly improved by cleaving peptide from the resin using a mixture of 9 mL of TFA, 0.5 mL of thioanisole, 0.3 mL of ethanediol, and 0.2 mL of anisole for 1 h.

Peptides with backbone *N*-methyl groups were synthesized manually according to the method of Biron et al. (19). Peptides with side chain methylations were synthesized on tBoc 4-methylbenzhydrylamine (MBHA) resin on a 0.25 mmol scale, either manually for peptides containing backbone *N*-methyl groups or using the synthesizer for peptides with no backbone *N*-methyl groups. Side chain *N*-methyl Gln residues were prepared by deprotecting Glu(tBu) side chains on resin (TFA/H₂O, 95:5, v:v) and then amidating (22 °C, overnight) under N₂ with 1 mmol of benzotriazole-1-yl-oxy-tris(dimethylamino)phosphonium hexafluorophosphate (BOP), 2 mL of 2.0 M dimethylamine in methanol, and 5 mL of dimethylformamide (DMF); this procedure was repeated for an additional 4 h. Although BOP is a less efficient

coupling agent than HATU [2-(7-aza-1*H*-benzotriazole-1-yl)-1,1,3,3-tetramethyluronium hexafluorophosphate], the latter reagent gave guanylation side products during long incubations. In one peptide, 5MeQ-PEG-5MeQ (see Figure 1A), a PEG moiety, Fmoc-8-amino-3,6-dioxaoctanoic acid ("Fmoc-mini-PEG", Peptides International), was incorporated into the middle of the peptide. After incorporation of the PEG group, the remaining amino acids were incorporated into the peptide as described above.

The MBHA resin was washed with DMF, and the peptide was cleaved and deprotected using anhydrous HF/*p*-cresol (10:1, v:v, 0 °C). After the peptides were precipitated in ice-cold diethyl ether, they were purified by using C18 preparative HPLC (Zorbax) at 22 °C, either with a water/acetonitrile (both 0.1% TFA, v:v) gradient or with an isocratic mixture. The peptide purity was $\geq 95\%$ as determined by analytical HPLC. Molecular masses of the peptides were verified with ESI- and MALDI-TOF mass spectrometry. A Lys residue was incorporated into all inhibitor peptides to aid cellular ingress of peptides (for studies not included herein) and possibly to increase solubility. The N-terminal *N*-methylantranilic acid was added to allow detection by fluorescence and UV spectroscopy.

Dissolving and Disaggregation of YAQ₁₂A: Sedimentation Assays of YAQ₁₂A Aggregation. Aggregation of YAQ₁₂A was assessed as the concentration of monomeric peptide remaining in solution after sedimentation, as described elsewhere (20). The elution of 100 μ M YAQ₁₂A via size exclusion chromatography was most consistent with the monomeric state. Chromatography was performed using a Superdex Peptide 10/300 GL column (GE Lifesciences) equilibrated with 10 mM sodium phosphate (pH 7.40); the flow rate was 0.5 mL/min (see Figure 2F,G). The apparent molecular weight (MW^{app}) was estimated on the basis of a calibration curve of molecular weight standards (Figure 4 of the Supporting Information). Additional size exclusion chromatography experiments are described below.

The concentration was determined by the absorbance at 274.6 nm, using an extinction coefficient (ϵ) of 1420 M⁻¹ cm⁻¹. The solution was diluted to 100 μ M with 10 mM sodium phosphate (pH 7.40) and incubated with or without inhibitor peptides for various times at 37 °C without agitation. After incubation, the mixture was centrifuged in an Airfuge ultracentrifuge (Beckman) at 98000*g* for 1 h at 22 °C. One hundred microliters of the top third of the resulting solution was injected onto an analytical C18 RP-HPLC column and followed by the absorbance at 220 nm. The concentration of YAQ₁₂A injected was calculated from the peak area data compared to a standard curve made from solutions of YAQ₁₂A of known concentrations. In more recent experiments, we were able to shorten the time between analyses by performing isocratic analyses; using a Zorbax C18 column, and a water/acetonitrile/TFA (87.5:12.5:0.1, v:v:v) eluent, YAQ₁₂A elutes at ~ 6 min and 5QMe₂ elutes at ~ 22 min (Figure 1 of the Supporting Information).

Stock solutions of inhibitor peptides at ~ 4 mM were made from pure lyophilized peptide and Milli-Q purified water, adjusted to 7.00, since the pH affects the ϵ of *N*-methylantranilic acid. The concentration of the stock was determined by the absorbance using an ϵ_{337} of 2690 M⁻¹ cm⁻¹. Aliquots at various concentrations were frozen, lyophilized, and stored at -20 °C. All fibrillation reactions were performed in siliconized microfuge tubes.

Additional Size Exclusion Chromatography Experiments. As stated above, initial experiments showed that

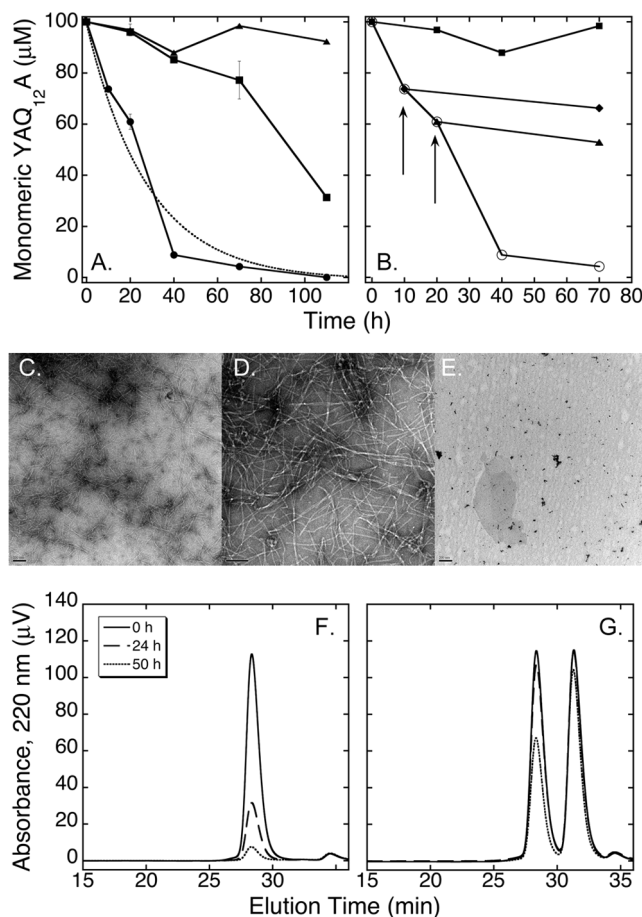


FIGURE 2: Time course of YAQ₁₂A aggregation and inhibition by 5QMe₂, electron microscopy of reaction products, and size exclusion chromatography of YAQ₁₂A in the absence or presence of 5QMe₂. (A) Aggregation of 100 μ M YAQ₁₂A in the absence of 5QMe₂ (○) or in the presence of 100 μ M (■) or 1.0 mM (▲) 5QMe₂ (mean \pm SD of three replicates). The dotted line represents a least-squares fit to a monoexponential equation. The amount of YAQ₁₂A remaining in solution at various time points in the incubation was measured using the sedimentation assay described in Experimental Procedures and originally described in ref 20. (B) Effect of adding 5QMe₂ to YAQ₁₂A at different points in the aggregation time course. 5QMe₂ (1 mM) was added to 100 μ M YAQ₁₂A at 0 h (■) or after YAQ₁₂A had been allowed to aggregate for 10 (◆) or 20 h (▲). (○) No inhibitor. Results are the amounts of monomeric YAQ₁₂A remaining in solution at various time points. (C–E) Electron micrographs of 100 μ M YAQ₁₂A incubated for 40 h at 37 °C in the absence (C and D) or presence (E) of 500 μ M 5QMe₂. No grossly visible precipitate was present for YAQ₁₂A incubated in the presence of inhibitor. The figures show 15000 \times magnification (C and E) or 49000 \times magnification (D), with scale bars of 100 nm (C and E) or 200 nm (D). (F and G) Size exclusion chromatography of 100 μ M disaggregated YAQ₁₂A alone (F) or in the presence of 170 μ M 5QMe₂ (G). Aliquots (100 μ L) of these solutions were chromatographed at 0, 24, and 50 h (black, blue, and red, respectively). Chromatography was performed using a Superdex Peptide 10/300 column; the effluent was 10 mM sodium phosphate containing 10 mM NaCl (pH 7.40), and the flow rate was 0.5 mL/min. Column effluent was monitored at 220, 230, 274, and 337 nm; the chromatograph shown was monitored at 230 nm. YAQ₁₂A elutes as a single peak with an elution time most consistent with an MW^{app} of ~ 1805.5 , close to the actual molecular weight of 1860. 5QMe₂ elutes somewhat later, at a position consistent with monomer ($MW^{app} \sim 1176.0$).

YAQ₁₂A, disaggregated as described above, eluted from a Superdex Peptide column in a position most consistent with a monomeric state. To examine the time course of this chromatographic behavior, and the effect of the aggregation inhibitor

peptide 5QMe₂ described in Results, we performed the following series of size exclusion chromatography experiments. A 100 μ M solution of freshly disaggregated YAQ₁₂A was chromatographed either alone or in the presence of 170 μ M 5QMe₂ [in other experiments, a 1:1 YAQ₁₂A:5QMe₂ molar ratio was used (see, for example, Figure 5 of the Supporting Information)]. To make the mixture of peptides, 5QMe₂ was dissolved in a water/TFA mixture (100:0.1, v:v) and distributed into siliconized microfuge tubes. Solvent was evaporated under a stream of N₂ followed by lyophilization. To the dry film were added YAQ₁₂A solutions. After incubation of these solutions at 37 °C for 0, 24, and 50 h, a 100 μ L aliquot of each solution was injected onto a Superdex Peptide 10/300 GL column. The mobile phase was 10 mM sodium phosphate containing 10 mM NaCl (pH 7.40). The flow rate was 0.5 mL/min. The column effluent was monitored at 220, 230, 274, and 337 nm. Essentially the same chromatographic pattern was observed at each wavelength, except that only 5QMe₂ could be observed at 337 nm, where the *N*-methyl anthranilate moiety absorbs.

Inhibition of Seeded YAQ₁₂A Fibril Growth by 5QMe₂. To produce fibril seeds, YAQ₁₂A fibrils were made by incubating a 250 μ M solution of the peptide, initially dissolved as described above, at 37 °C for at least 1 week. Immediately prior to the seeding experiment, the seed slurry was sonicated for 5 min using a Bransonic ultrasonic bath (model 2510R-MT, Branson Ultrasonics Corp.). In preliminary experiments, we assessed the effects of addition of various nominal concentrations of YAQ₁₂A fibril seeds to a fresh, 100 μ M solution of YAQ₁₂A (see Figure 2A of the Supporting Information; Figure 2B of the Supporting Information shows that the seeds were indeed fibrillar). The nominal concentration of the seed slurry was defined from the original peptide concentration of the solution from which the seed slurry was made. From these experiments, we determined that a nominal concentration of 8 μ M was optimal for this batch of seed fibrils for the observation of both accelerated fibrillation of fresh YAQ₁₂A and the effects of 5QMe₂ on seeded fibril growth.

For the seeding experiments, we compared YAQ₁₂A fibrillation in the presence or absence of fibril seeds and in the presence or absence of 5QMe₂. YAQ₁₂A was freshly disaggregated and dissolved in 10 mM phosphate (with 1 μ M NaN₃) to a concentration of approximately 150 μ M. The actual concentration was determined by the absorbance at 274.6 nm and confirmed by injection of an aliquot onto an analytical C18 RP-HPLC column, as described above. Siliconized microfuge tubes were prepared with or without a sufficient amount of 5QMe₂ so that the final concentration of this peptide would be 100 μ M. To this mixture, sufficient buffer was added so that the total final volume would be 600 μ L and the final YAQ₁₂A concentration would be 100 μ M. Lastly, an aliquot of the fibril seed slurry described above was added to some samples to give a final nominal seed concentration of 8 μ M. Thus, in those samples containing 5QMe₂, the YAQ₁₂A:5QMe₂ molar ratio was 1:1. The mixtures were incubated at 37 °C for 0, 5, 24, or 50 h. At each time point, fibrillation was assessed by the sedimentation assay described above, performed at least in triplicate; results are reported as means \pm SD.

Electron Microscopy. Electron microscopy was performed as described elsewhere (16); micrographs were recorded at magnifications of 15000 \times or 39000 \times , plus 1.4 \times magnification from the CCD camera.

Surface Plasmon Resonance. YAQ₁₂A that had been disaggregated and centrifuged as described previously (20) was

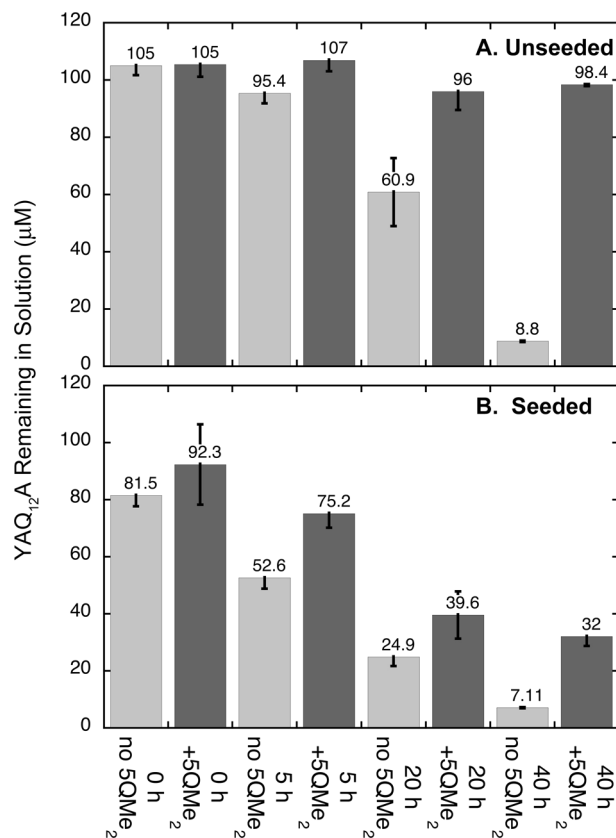


FIGURE 3: Effect of 5QMe₂ on seeded and unseeded fibrillation of YAQ₁₂A. (A) A freshly disaggregated, 100 μ M solution of YAQ₁₂A was incubated in the presence or absence of 100 μ M 5QMe₂, as described in Experimental Procedures, and then was assayed for YAQ₁₂A remaining in solution at 0, 5, 20, and 40 h. (B) A freshly disaggregated, 100 μ M solution of YAQ₁₂A was incubated with preformed YAQ₁₂A fibril seeds at a nominal concentration of 8 μ M (i.e., 100:8 seed YAQ₁₂A:soluble YAQ₁₂A molar ratio), in the presence or absence of 100 μ M 5QMe₂, as described in Experimental Procedures, and the YAQ₁₂A remaining in solution was assayed as described for panel A. Results are means \pm SD of three determinations, reported in micromolar YAQ₁₂A remaining in solution.

immobilized on a CM5 sensor chip using standard amine coupling procedures, as described in the manufacturer's instructions (Pharmacia Biosensor AB). All assays were conducted using a Biacore 3000 instrument at 25 °C, at a flow rate of 20 μ L/min, with association and dissociation times of 120 s, in HSP-B buffer (Biacore). Each concentration of analyte was tested in triplicate. Kinetic data were analyzed first using BIA evaluation software (Biacore) and then by nonlinear least-squares analysis using Kaleidagraph and using a nonlinear least-squares fitting program described by Yamaoka et al. (21). Adsorption kinetics were fitted as a bimolecular interaction of the analyte (5QMe₂) interacting with the immobilized ligand (YAQ₁₂A), forming the 1:1 complex at the sensor surface. The best fit (see below, Figure 3) was obtained with single-exponential equations for association and dissociation. Specifically, during association, the SPR signal varied with time as given by the equation

$$R_t = \frac{k_{\text{on}}[I]B_{\text{max}}}{k_{\text{on}}[I] + k_{\text{off}}} [1 - e^{-(k_{\text{on}}[I] + k_{\text{off}})t}] \quad (1)$$

where R_t is the SPR signal ("response units" or RUs) as a function of time, k_{on} and k_{off} are association and dissociation constants, respectively, B_{max} is the maximum binding capacity, and t is the

time in seconds. Similarly, during dissociation, the SPR signal varied according to the equation

$$R_t = R_{eq}(e^{-k_{off}t}) \quad (2)$$

where R_{eq} is the signal reached at equilibrium. Both equations, for association and dissociation, are as described by DeMol and Fischer (22). Figure 3 represents a global fit of all data using single values for k_{on} and k_{off} . The dissociation constant, K_d , was calculated as k_{off}/k_{on} .

Circular Dichroism. Circular dichroism (CD) spectra were recorded using an AVIV 202 spectropolarimeter. Lyophilized inhibitor peptides were dissolved directly in 10 mM phosphate buffer (pH 7.40). Monomeric 50 μ M YAQ₁₂A was prepared as described above in the same buffer. Spectra were recorded at 22 °C, with a 1 mm cuvette; five scans were averaged, and contributions from buffer were subtracted. Data were smoothed using a macro in Kaleidagraph.

Fibril film CD spectra were measured essentially as described by Darnell et al. (12). Briefly, we obtained a concentrated slurry of fibrils by first centrifuging the slurry in a microfuge for 5 min and resuspending the pellet in the same buffer; 20 μ L aliquots of the slurry in 5 μ L droplets were placed onto cut quartz plates [12.5 mm \times 12.5 mm (Starna)] and allowed to coalesce into one aqueous film. All samples were dried under vacuum overnight at room temperature. Spectra were recorded immediately after the plates had been removed from vacuum, using an Aviv (Lakewood, NJ) model 202 spectropolarimeter at 1 nm intervals from 260 to 190 nm with an averaging time of 1 s, with a bandwidth of 1 nm, and at 25 °C. To determine whether linear dichroism was present, spectra were again recorded after the plates were rotated by 90°. Any samples that exhibited shifts in maxima or minima were discarded from the data set. Data sets showing scatter after 90° rotation were still used. Spectra shown in Results represent the averages of five scans for each film. Spectra are presented as wavelength versus background-corrected raw ellipticity signal.

Experimental Procedure for Analytical Ultracentrifugation. Equilibrium sedimentation analytical ultracentrifugation was performed using a Beckman Optima XLA ultracentrifuge equipped with an An-60Ti rotor with six-sector cells. Solutions of monomeric 100 μ M YAQ₁₂A were prepared as described above in 10 mM sodium phosphate (pH 7.40). This peptide sample was added to lyophilized aliquots of 5QMe₂, yielding final inhibitor concentrations of 100 μ M (1:1 YAQ₁₂A:5QMe₂ molar ratio), 500 μ M (1:5 YAQ₁₂A:5QMe₂ molar ratio), and 1 mM (1:10 YAQ₁₂A:5QMe₂ molar ratio). Of the four cells in the rotor, one contained buffer only [10 mM sodium phosphate (pH 7.40)], two were duplicates, each containing the three mixtures of YAQ₁₂A and 5QMe₂ described above, while the last contained samples of 5QMe₂ alone at 100 μ M, 500 μ M, and 1 mM. Sedimentation was monitored at 230 and 280 nm, at 20 °C, with 1 h between scans. The rotor speed progressed from 3000 rpm (1 scan) to 36000 rpm (16 scans) to 48000 rpm (13 scans) to 60000 rpm (19 scans). Equilibrium was demonstrated by the absence of change in the absorbance profile over the course of at least 8 h.

Sedimentation equilibrium analytical ultracentrifugation data were analyzed using an approach that derives in part from previous methods for the analysis of the formation of complexes by two dissimilar species, interacting at sedimentation equilibrium in an ultracentrifugal field (23–26). Absorbances used for analysis were at 280 nm, except 5QMe₂ alone at 100 μ M, which

was followed at 230 nm for greater sensitivity at the lower concentration. Additional details of analysis, including derivation of equations, and methods for determination of \bar{v} (27), are given in the Supporting Information.

RESULTS

Sedimentation Screening Assays. To screen peptides as potential polyQ fibrillation inhibitors, we used YAQ₁₂A, a synthetic polyQ peptide that forms fibrils over the course of several days, making it amenable to kinetic analysis. In addition, in contrast to longer polyQ peptides, YAQ₁₂A can be highly purified. Thus, our assay consisted of measuring fibrillation in the presence and absence of potential inhibitor peptides. The potential inhibitors tested are shown in Figure 1A. Fibrils of short polyQ peptides such as YAQ₁₂A cause very little or no appreciable thioflavin T fluorescence, however. For this reason, we used sedimentation assays (20) to follow the aggregation of YAQ₁₂A in the presence and absence of inhibitor peptides. For the purpose of performing screening assays, high inhibitor concentrations were used (4 mM inhibitor and 0.1 mM YAQ₁₂A). In the absence of inhibitors, after incubation of 100 μ M YAQ₁₂A for 40 h at 37 °C, 8.8 ± 0.3 μ M (mean \pm SD) monomer remained in solution (Figure 1B).

The first inhibitor tested was 5MeQMe₂, which contained both backbone and side chain glutamine N-methylations to disrupt hydrogen bonds at both locations. Alternate residues were modified to leave some amides available for binding to YAQ₁₂A (16, 17). This peptide and subsequent ones discussed in this paper also contain additional moieties, as in our earlier studies of inhibitors of β -amyloid and human prion peptide (PrP_{106–126}) aggregation (16, 17). *N*-Methylantranilic acid was added for fluorescence detection in cellular studies (not discussed herein); the single Lys residue and C-terminal carboxamidation are also used to favor ingress of the peptides into cells (17), and the Lys residue may also increase solubility.

Although incubation of 5MeQMe₂ with YAQ₁₂A did exhibit significant inhibition [36.8 ± 3.7 μ M monomeric YAQ₁₂A remaining in solution (Figure 1B)], this inhibitor was considerably less effective than expected, given that it was present at a 40:1 molar concentration relative to YAQ₁₂A.

We then attempted to optimize the inhibitor. Lengthening the core glutamine sequence from five residues to seven (7MeQMe₂) resulted in a less effective inhibitor (24.7 ± 1.7 μ M). On the basis of the hypothesis that methylating both side chain and backbone amides might hinder binding of the inhibitor to YAQ₁₂A, we synthesized 5MeQ, which has only backbone N-methylations. 5MeQ proved to be slightly more effective than the other inhibitors (42.2 ± 1.7 μ M). We also attempted to model a proposed polyQ fibril structure (8, 9) by connecting two 5MeQ peptides either with a tight β -hairpin turn (^DPro-Gly sequence) or with a flexible linker (PEG). These peptides were moderately effective as inhibitors, yielding 31.6 ± 1.0 and 51.5 ± 4.0 μ M monomeric YAQ₁₂A remaining in solution, respectively.

Surprisingly, 5QMe₂, with only side chain methyl groups (again, on alternate residues), completely inhibited aggregation of YAQ₁₂A, with essentially all of the YAQ₁₂A remaining in solution at the end of the incubation (91 ± 0.6 μ M). (QMe₂)₅, with side chain methylations on all Q residues, was less effective (58.9 ± 0.9 μ M monomeric YAQ₁₂A remaining) than 5QMe₂, demonstrating the importance of the alternating pattern of methylated residues. Finally, the unmethylated peptide, 5Q, was not inhibitory; after incubation of 5Q with YAQ₁₂A, the

concentration of the latter peptide remaining in solution was $11.9 \pm 1.7 \mu\text{M}$, similar to that of YAQ₁₂A alone.

Time Course of Inhibition of YAQ₁₂A Aggregation by 5QMe₂ and Electron Microscopy of Reaction Products. We then focused on 5QMe₂, by far the most effective of these inhibitors. Size exclusion chromatography confirmed that the top ultracentrifugal fraction of disaggregated YAQ₁₂A used for these assays was most consistent with a monomeric molecular weight (Figure 2F,G; see also Figure 4A,B of the Supporting Information). Sedimentation assays showed that the YAQ₁₂A monomer shows a monoexponential decline over 110 h, without a lag period [$k = 0.04 \text{ h}^{-1}$ (Figure 2A)]. When 100 μM YAQ₁₂A was incubated with 100 μM 5QMe₂, we observed a lag period, in which the level of soluble YAQ₁₂A declined slowly, followed by more rapid loss of this peptide from solution after ~ 70 h. When 100 μM YAQ₁₂A was incubated with 1 mM 5QMe₂, no aggregation was observed for the entire time period. Electron microscopy confirmed the sedimentation assay results. Incubation of YAQ₁₂A with 5QMe₂ (500 μM , for Figure 2E) abrogates fibril formation at 40 h.

As stated, in the absence of inhibitor, much of the YAQ₁₂A initially in solution precipitated and formed fibrils. As shown in panels F and G of Figure 2, however, at 0, 24, and 50 h, essentially all of the YAQ₁₂A in solution eluted from the size exclusion chromatography column at a position most consistent with a monomeric molecular weight. If any oligomeric YAQ₁₂A was in solution at these three times, it represents a very small and probably kinetically transient fraction of the total YAQ₁₂A in solution. The effect of adding 5QMe₂ to YAQ₁₂A was to keep the latter peptide in solution for a longer period of time, but 5QMe₂ did not alter the chromatographic behavior of YAQ₁₂A. As shown in Figure 2G, at increasing times, more YAQ₁₂A remained in solution in the presence than in the absence of 5QMe₂. The chromatographs show two well-resolved peaks, one each in the positions previously observed for YAQ₁₂A and 5QMe₂. In the presence of 5QMe₂, essentially all of the YAQ₁₂A was still in solution at 24 h, as shown by the fact that the size of the peak was essentially unchanged from that after 0 h. At 50 h, the YAQ₁₂A peak was slightly smaller than that seen at 0 or 24 h, but no additional peaks were observed. We demonstrate below that these two peptides form a complex, with a K_d of $\sim 1 \mu\text{M}$. The absence of a peak for this complex is consistent with dissociation of a complex of this affinity during chromatography.

Effect of Adding Inhibitor at Various Points in the Time Course of Aggregation. Many aggregating peptides are believed to form fibrils by a rate-limiting nucleation step followed by elongation of the nucleus (3, 5, 28, 29). To learn whether 5QMe₂ could prevent aggregation of YAQ₁₂A when added at different stages during a 70 h period of fibril formation, we added 1 mM 5QMe₂ to 100 μM YAQ₁₂A 10 or 20 h after the start of the incubation (Figure 2B). Monomeric YAQ₁₂A remaining after 70 h was then assessed by a sedimentation assay. 5QMe₂ was able to prevent all but a modest further decline in monomer concentrations, regardless of the time of addition. These experiments suggest that 5QMe₂ may act to disrupt both nucleation and elongation steps and maintain YAQ₁₂A in its monomeric state. The inhibitor did not reverse aggregation, however, as no additional monomer appeared in solution after incubation of the mixture with the inhibitor.

Inhibition of Seeded YAQ₁₂A Fibril Growth by 5QMe₂. These experiments were designed to assess whether 5QMe₂ could inhibit precipitation of YAQ₁₂A from solution in the presence of

Table 1: Inhibition of YAQ₁₂A by 5QMe₂ at Various Concentration Ratios

[5QMe ₂] (mM)	5QMe ₂ :YAQ ₁₂ A concentration molar ratio ^a	YAQ ₁₂ A monomer remaining
4.00	40	91.3 \pm 0.6
1.00	10	87.9 \pm 0.3
0.50	5	95.2 \pm 0.4
0.10	1	85.2 \pm 0.4
0.05	0.5	90.1 \pm 1.5
0.025	0.25	42.0 \pm 0.8
0.01	0.1	36.3 \pm 11.4

^aIn all cases, the YAQ₁₂A concentration was 100 μM at the start of the reaction. Incubation was conducted for 40 h at 37 °C. The monomeric YAQ₁₂A remaining in solution after the incubation was measured by RP-HPLC, as described in Experimental Procedures.

preformed fibril seeds. The results shown in panels A and E of Figure 2 indicate that 5QMe₂, when added to YAQ₁₂A at the start of a fibrillation reaction, can act as a nucleation inhibitor. That is, 5QMe₂ can prevent or delay the growth of fibrils under unseeded fibrillation conditions. The data shown in Figure 2B suggest that 5QMe₂ can also act as a fibril extension inhibitor, since addition of 5QMe₂ 10 or 20 h after the start of the reaction prevented nearly all additional precipitation of YAQ₁₂A from solution. To test further the idea that 5QMe₂ can act as a fibril extension inhibitor, we examined the seeded growth of YAQ₁₂A. In particular, preformed fibril seeds were added to disaggregated solutions of YAQ₁₂A, with or without 5QMe₂, as described in Experimental Procedures. As a control experiment, the same incubations were performed without the addition of YAQ₁₂A seeds. The results of these experiments are shown in Figure 3. The data in Figure 3A for unseeded fibril growth are similar to those shown in Figure 2: in unseeded, freshly disaggregated solutions of YAQ₁₂A, the peptide spontaneously precipitates and forms fibrils, and the addition of 5QMe₂ inhibits fibrillation, causing the YAQ₁₂A to remain in solution. When YAQ₁₂A fibrils are added to fresh, disaggregated solutions of YAQ₁₂A (Figure 3B), more YAQ₁₂A is lost from solution at each time point than in the absence of added seeds. Thus, the added fibrils do indeed seed fibrillation. When 5QMe₂ is also added to the mixture of fibril seeds and fresh YAQ₁₂A solutions, it inhibits the loss of soluble YAQ₁₂A into the insoluble fraction. Since the addition of fibril seeds largely bypasses nucleation, these data indicate that 5QMe₂ inhibits fibril extension. Thus, 5QMe₂ is both a nucleation and fibril extension inhibitor.

Inhibitor Concentration Dependency. We examined the inhibitor concentration dependency using sedimentation assays. YAQ₁₂A (100 μM) was incubated for 40 h with various concentrations of 5QMe₂, at molar ratios ranging from 40:1 to 1:10 (5QMe₂:YAQ₁₂A), and after ultracentrifugation, the top fraction was assayed for soluble YAQ₁₂A. As shown in Table 1, inhibition was essentially complete at ratios of 1:1 but was significant even at a substoichiometric ratio of 1:10 (5QMe₂:YAQ₁₂A).

Kinetics of YAQ₁₂A and 5QMe₂ Binding, As Assessed by Surface Plasmon Resonance (SPR). After observing that 5QMe₂ could inhibit aggregation of YAQ₁₂A at substoichiometric levels, we investigated the affinity and kinetics of YAQ₁₂A and 5QMe₂ binding with surface plasmon resonance (SPR). We reasoned that 5QMe₂ could act at substoichiometric ratios by interacting transiently and sequentially with monomeric YAQ₁₂A molecules. SPR experiments showed rapidly reversible

binding and dissociation of 5QMe₂ to immobilized YAQ₁₂A over a range of inhibitor concentrations. Figure 4A shows a global fit of the data to monoexponential rate equations (described in Experimental Procedures); Figure 4B shows residuals (differences between experimental values and theoretical fits). From these analyses, k_{on} and k_{off} for each set of triplicate runs were 0.026 $\mu\text{M s}^{-1}$ and 0.024 s^{-1} , respectively, yielding a value of 0.92 μM for K_d . Data for individual curves were also analyzed

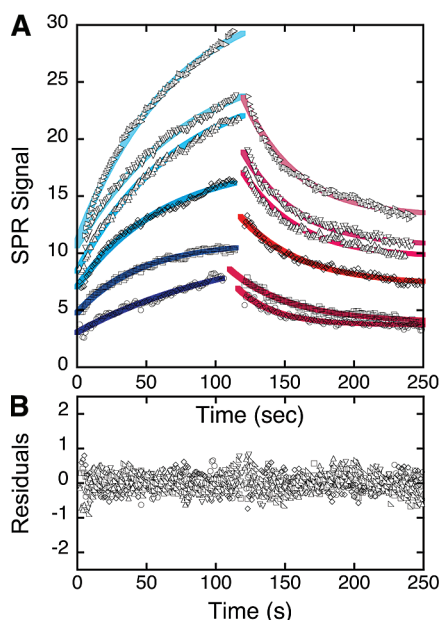


FIGURE 4: Surface plasmon resonance of immobilized YAQ₁₂A interacting with soluble 5QMe₂. (A) SPR data showing binding and subsequent dissociation of 5QMe₂ at various concentrations, ranging from 5 to 50 μM , to and from immobilized YAQ₁₂A. In the figure, points represent experimental data and solid lines are non-linear least-squares fits of the data to monoexponential kinetics of binding and desorption. (B) Residuals were calculated as the difference between experimental data and calculated values using the parameters obtained from nonlinear least-squares fits. For both panels, the concentrations of 5QMe₂ were as follows: (○) 5, (□) 10, (◇) 20, (Δ) 30, (▽) 40, and (right-pointing triangles) 50 μM .

using the same equations, and the values obtained for k_{on} , k_{off} , and K_d (representing an arithmetic mean of the values) were 0.030 $\mu\text{M s}^{-1}$, 0.026 s^{-1} , and 0.87 μM , respectively, in reasonable agreement with the values obtained from global fitting. These data indicate very rapid association and dissociation of predominantly a 1:1 complex of YAQ₁₂A and 5QMe₂, and moderate affinity. The rapidity of binding and dissociation is reminiscent of chaperones, which act substoichiometrically by making rapid, transient complexes with sequential molecules of their targets.

AUC and Complex Stoichiometry. We used sedimentation equilibrium analytical ultracentrifugation experiments to analyze the complex (IQ) formed from YAQ₁₂A (Q) and 5QMe₂ (I). We first demonstrated that the inhibitor alone is monomeric at three concentrations (100, 500, and 1000 μM) and at three rotor speeds (Figure 5). The experimental molecular weight (mean \pm SD for all of the conditions described above) for 5QMe₂ at these concentrations was 975.2 ± 32.1 , very close to the expected value of 976. When the results for the three concentrations were analyzed globally, the molecular weights obtained were 988.5, 1000.0, and 980.1 for rotor speeds of 36000, 48000, and 60000 rpm, respectively. This is again in agreement with the expected molecular weight for 5QMe₂.

The complex formed between I and Q was analyzed using the experimental procedures described by Winzor et al. (23), which is based on earlier papers by the same group (24–26). A description of this technique, including derivations of equations as used in the experiments on these particular peptides, is given in detail in the Supporting Information. Briefly, sedimentation equilibrium data are analyzed according to the equation

$$A_i(r) = C_I(r_F)\epsilon_I\psi_I(r) + C_Q(r_F)\epsilon_Q[\psi_I(r)]^p + C_{IQ}(r_F)\epsilon_{IQ}[\psi_I(r)]^{p+1} + C_{I_2Q}(r_F)\epsilon_{I_2Q}[\psi_I(r)]^{p+2} + \dots \quad (3)$$

where $C_i(r)$ is the concentration of each species at each radial position, r , in the ultracentrifugal field. The function $\psi_i(r)$ is defined as $\exp[M_i\phi_i(r^2 - r_F^2)]$, where $\phi_i = [(1 - \bar{v}_i\rho)\omega^2]/(2RT)$. M_i is the molecular weight of each species. r_F is an arbitrarily chosen fixed radial distance from the center of rotation. \bar{v} is the partial

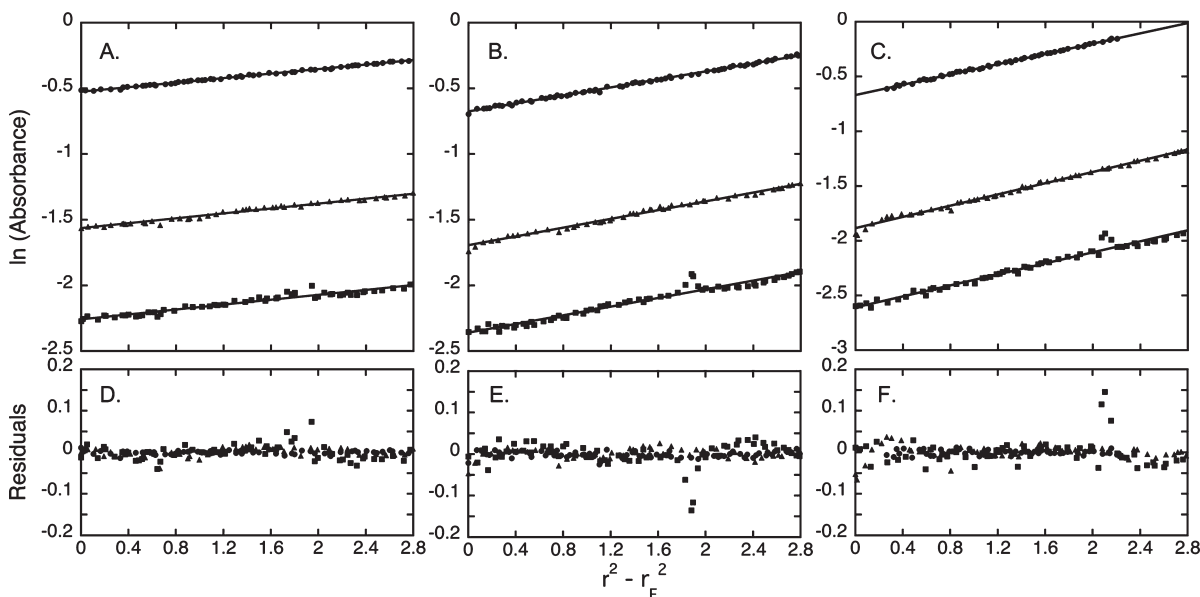


FIGURE 5: Sedimentation of 5QMe₂ alone, at 100 (■), 500 (▲), and 1000 μM (●) and at 36000 (A), 48000 (B), and 60000 rpm (C). Conditions were as described in Experimental Procedures.

specific volume of each species. ω is angular velocity. ρ is solvent density. T is the temperature (kelvin). R is the gas constant. For synthetic peptides, the values of M_i are known: $M_I = 976$, $M_Q = 1860$, $M_{IQ} = 2736$, etc., for other types of complexes. The parameter p is defined as $M_i\phi_i/M_j\phi_j$; in our experiments, i is Q and j is I, and thus, $p = 1.90$.

In these experiments, sedimentation equilibrium ultracentrifugation was performed using three sets of peptide concentrations, either an equimolar concentration of I and Q (100 μ M each) or an excess of the inhibitor (500 or 1000 μ M I with 100 μ M Q). In addition, the sample was centrifuged to equilibrium at three angular velocities, 36000, 48000, and 60000 rpm. It was necessary to use an equimolar or higher inhibitor concentration because at lower concentrations of the inhibitor, Q would not stay in solution, as is also indicated in Figure 2.

The null hypothesis to be tested in these experiments is that, in agreement with SPR data, the predominant complex between I and Q is a 1:1 complex. Under the conditions used in these experiments (equimolar or excess I compared to Q) and given the K_d (0.92 μ M) obtained from SPR, the expected concentration of Q is low compared to those of either I or IQ, and also with respect to the experimental error in the measurement of absorbance. For this reason, the results were analyzed in two, complementary ways, as follows.

First, the data were analyzed according to eq 3, and the value of K_d was evaluated from the values of the three parameters, $C_I(r_F)$, $C_Q(r_F)$, and $C_{IQ}(r_F)$. Second, we used the value of K_d obtained from SPR experiments to calculate the least precise (because it has the lowest value) of the three parameters mentioned above, $C_Q(r_F)$. In other words, in the second procedure, data were analyzed by nonlinear least-squares methods, using the equation

$$A_I(r) = \frac{C_I(r_F)}{\varepsilon_I} \psi_I + \frac{\frac{C_I(r_F)}{\varepsilon_I} K_d}{\frac{C_{IQ}(r_F)}{\varepsilon_{IQ}}} \psi_I^p + \frac{C_{IQ}(r_F)}{\varepsilon_{IQ}} \psi_I^{p+1} \quad (4)$$

Figure 6 shows the results of these analyses. In the figure, the symbols are experimental data points, the thin black line is the analysis of the data using eq 3, and the somewhat thicker gray line represents the fit of the data using eq 4. As shown in the figure, the two fits are essentially superimposable. A mean value (\pm SD) of $0.74 \pm 0.22 \mu$ M was obtained for K_d from the values of $C_I(r_F)$, $C_Q(r_F)$, and $C_{IQ}(r_F)$, which is in reasonable agreement with the value for K_d obtained from SPR of 0.92 μ M.

The analysis also indicated that nearly all of the Q (YAQ₁₂A) remaining in solution is part of a complex. Although additional terms, corresponding to higher-order complexes, could be added to the equation to fit the data, such terms did not improve the fit (Figure 3 of the Supporting Information). Because the theoretical fits overlap completely and are indistinguishable from that obtained using the simpler equation, it is most parsimonious to conclude that the predominant complex is a 1:1 stoichiometric complex, also in agreement with SPR data. Finally, as discussed in the Supporting Information, the fit of data to the model containing a complex was compared to that containing no complex, by using the Akaike Information Criterion [AIC (21, 30)]. The AIC is a measure of the goodness of fit of an estimated statistical model that rewards goodness of fit (as determined by the sum of squares or χ^2) and also penalizes the number of parameters and therefore penalizes overfitting. Thus, in general, a lower AIC

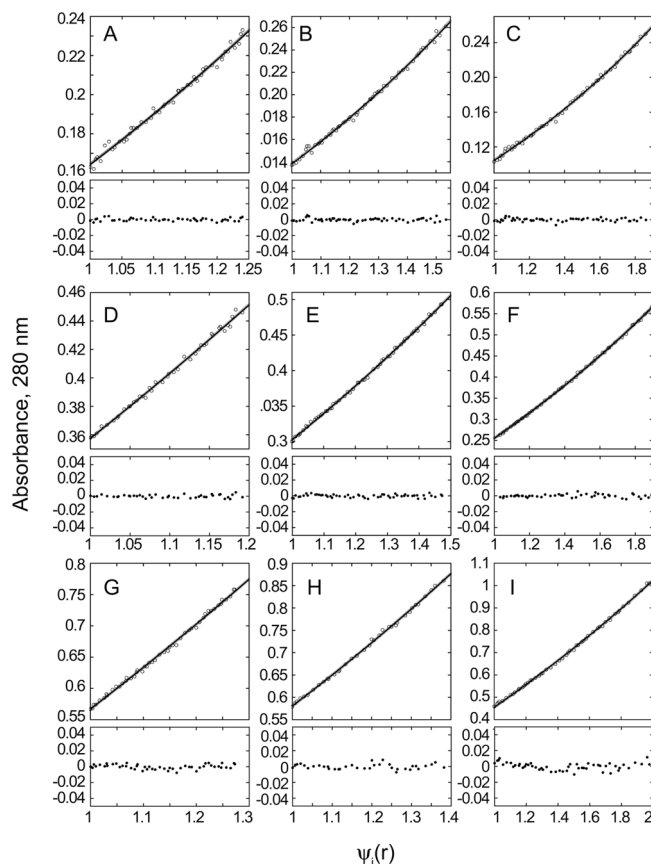


FIGURE 6: Sedimentation equilibrium analytical ultracentrifugation of YAQ₁₂A/5QMe₂ mixtures. The figure shows data for mixtures of 100 μ M YAQ₁₂A and 100 (A–C), 500 (D–F), or 1000 μ M 5QMe₂ (G–I) centrifuged to equilibrium at 36000 (A, D, and G), 48000 (B, E, and H), or 60000 rpm (C, F, and I). Concentrations were monitored by the absorbance at 230 nm (A–C) or 280 nm (D–I) to obtain the desired level of sensitivity. The symbols are experimental data points; the thin black line is the analysis of the data using eq 3, and the thicker gray line represents the fit of the data using eq 4. For all panels, the bottom graph shows residual values, calculated as the difference between experimental and theoretical values calculated from the parameters obtained from nonlinear least-squares fits.

indicates a preferable model, i.e., the best fit of the data with a minimum number of free parameters. As indicated in Table 1 of the Supporting Information, in all cases but one (which was a virtual tie), the inclusion of a term for a 1:1 complex, rather than only free I and free Q, lowered the AIC, indicating that this was a preferable model. In conclusion, the analytical ultracentrifugation data are consistent with a model in which YAQ₁₂A forms mainly a 1:1 complex with 5QMe₂.

Secondary Structure of 5QMe₂ and Related Peptides. The CD spectrum of YAQ₁₂A in solution shows a small maximum at \sim 220 nm and a trough with a minimum at \sim 199 nm, consistent with a PPII-like helical structure (Figure 7A). When it forms fibrils, it undergoes a transition to β -sheet structure, as shown by film CD spectroscopy (Figure 7B), as do other short polyQ peptides (12, 31–34). The CD spectrum of 5QMe₂ is also consistent with a left-handed, PPII-like structure (Figure 7A), though with a red-shifted maximum at \sim 232 nm, and a minimum at \sim 199 nm, possibly suggesting subtle structural differences from YAQ₁₂A. In contrast to 5QMe₂, two of the less effective inhibitors, 5MeQ and 5MeQMe₂ with backbone N-methylation, had CD spectra indicative of β -sheet (Figure 7C). These data suggest that the most effective inhibitor has a structure resembling the soluble

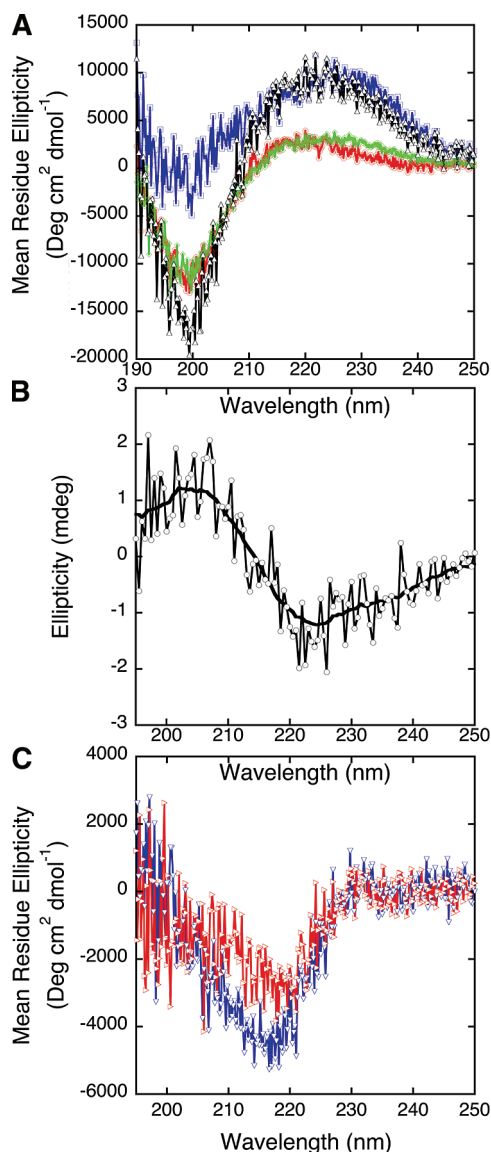


FIGURE 7: (A) CD spectroscopy of YAQ₁₂A, 5QMe₂, and an equimolar mixture of the two peptides. Circular dichroism spectra of YAQ₁₂A [100 μ M (red circles)], 5QMe₂ [100 μ M (blue squares)], and an equimolar mixture of the two peptides [each peptide at 100 μ M (green diamonds)]. Also shown is a calculated weighted mean of the two spectra of YAQ₁₂A and 5QMe₂ alone (black triangles). Points are experimental data; lines represent curves smoothed using the smooth macro of Kaleidagraph. For the sake of clarity, only every third point is shown in the figure. (B) Circular dichroism spectrum of YAQ₁₂A fibril films. The procedure was essentially that described by Darnell et al. (12). (C) CD spectra of 5MeQ (blue triangles) and 5MeQMe₂ (red triangles) under the same conditions described for panel A.

form of its PPII target peptide, YAQ₁₂A, while the less effective inhibitors have the structure, β -sheet, of the final fibrillar product of the aggregation pathway. A 1:1 mixture of YAQ₁₂A and 5QMe₂ did not match an arithmetic weighted mean of the spectra of the two individual peptides (Figure 7A), which is consistent with observations that the two peptides form a distinct complex mentioned above.

DISCUSSION

In this paper, we have described N-methylated inhibitors of polyQ peptide aggregation. 5QMe₂, with only alternate side chain amides N-methylated, was far more effective than the

others, including 5MeQ with only backbone N-methylations and 5MeQMe₂ with both backbone and side chain N-methylation. These results demonstrate the importance of side chain hydrogen bonding in polyglutamine fibrillation, which has been posited from molecular modeling (35, 36). Also, the inhibitor in which alternate side chains were methylated (5QMe₂) was more effective than that in which all the side chains were methylated [(QMe₂)₅], indicating the need to retain some unmodified amides for binding to the aggregating target peptide.

Addition of 5QMe₂ to YAQ₁₂A at stoichiometric or higher ratios prevented the disappearance of monomeric YAQ₁₂A from solution for 40 h, although at 70 h, complete inhibition required higher stoichiometric ratios (e.g., 10:1 5QMe₂:YAQ₁₂A). These results suggest that 5QMe₂ inhibits nucleation of YAQ₁₂A but does not eliminate it. In addition, adding 5QMe₂ to solutions of YAQ₁₂A at various times after the start of fibrillation prevented all but a minor degree of further aggregation of YAQ₁₂A for times up to 70 h, suggesting that 5QMe₂ also inhibits fibril elongation. Furthermore, 5QMe₂ inhibited seeded fibrillation of YAQ₁₂A, which largely bypasses nucleation steps, suggesting that 5QMe₂ is a fibril extension as well as a nucleation inhibitor. 5QMe₂ causes YAQ₁₂A to remain in a monomeric state rather than that of a soluble multimer. Thus, it is more properly called an aggregation inhibitor, rather than a fibrillation inhibitor.

SPR indicates very rapid binding and dissociation of a 1:1 complex, with moderate affinity ($K_d = 0.92 \mu$ M). Both SPR and sedimentation equilibrium analytical ultracentrifugation suggest that the predominant complex formed by 5QMe₂ and YAQ₁₂A has a 1:1 stoichiometry. The rapidity with which the complex dissociated was also shown by size exclusion chromatography, where both 5QMe₂ and YAQ₁₂A eluted at a position most consistent with the monomeric MW^{app}. Chromatography of a mixture of these peptides yielded two peaks, in the same elution positions as the individual peptide, indicating complete dissociation of the complex during the chromatography (for further discussion of this point, see the text and Figure 4A,B of the Supporting Information). This binding pattern of target peptides is reminiscent of that of chaperone proteins, which also bind their targets with moderate affinity but have very high k_{on} and k_{off} values. Rates have been measured for Hsp70 and Hsp90 (37, 38) (though these particular chaperonins do not bind polyQ peptides). Although it is sometimes assumed that a high affinity indicates a better aggregation inhibitor, this is not necessarily the case. 5QMe₂ is notable for acting at substoichiometric levels, suggesting that the kinetics of complex association and dissociation are faster than the kinetics of YAQ₁₂A aggregation. Thus, the effectiveness of 5QMe₂ is likely due to fast k_{on} and k_{off} rates and could be hampered by a higher affinity.

Thus, 5QMe₂, like chaperones, may keep aggregation-prone peptides or proteins in a less aggregation-prone conformation, e.g., by preventing β -sheet formation. Indeed, CD spectroscopy shows that 5QMe₂ does not have a β -strand structure. Rather, its spectrum is most consistent with a PPII helical conformation. In contrast, the backbone-modified peptides, 5MeQ and 5MeQMe₂, showed β -strand structure by CD (Figure 7C) and were less effective inhibitors than 5QMe₂. It is striking that the secondary structure of 5QMe₂ resembles that of its target peptide, a property that may be generalizable to all N-methylated inhibitors. Indeed, when we added 5QMe₂ to YAQ₁₂A, both reactants had structures consistent with PPII or PPII-like helices as determined by CD spectroscopy (although not identical CD spectra), and the products in the mixture also had a PPII

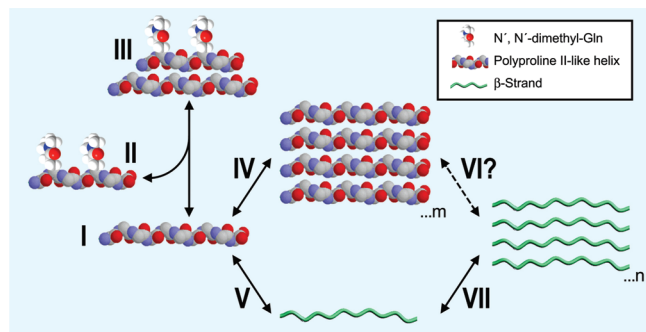


FIGURE 8: Schema depicting the model of inhibition of polyQ aggregation by 5QMe₂. YAQ₁₂A has PPII-like structure in solution (I), as do other polyQ peptides (12, 31–34). 5QMe₂ (II) also has a PPII-like conformation and is predominantly or entirely monomeric in solution. 5QMe₂ rapidly binds YAQ₁₂A and forms transient complexes (III). PolyQ peptides have been shown to form oligomers with a PPII-like conformation [IV (18)], and it is not known whether these are on- or off-pathway for fibril formation (VI). Monomeric YAQ₁₂A could also undergo a PPII to β -strand transition (V), which has been proposed for other polyQ peptides (31–34), and these could self-associate into fibrils (VII). The inhibitor is chaperone-like in that it binds and releases its target very rapidly, which is presumably more rapid than nucleation of YAQ₁₂A itself. The side chain *N*-methyl groups of 5QMe₂ result in the formation of predominantly 1:1 stoichiometric complexes with YAQ₁₂A, blocking oligomerization of the peptides in this complex, and delaying the transition from PPII to β -strand or β -sheet.

structure. Similarly, inhibitors of A β aggregation, such as the backbone *N*-methylated peptide, A β 16–20m (16, 17), have similar secondary structure as their targets, but in those cases, β -sheet.

These results are consonant with our recent observations (18) that short peptides containing a QQQ triplet aggregate into soluble oligomeric species as PPII helices, although they are too short ever to form fibrils or adopt a β -sheet structure. Longer polyQ peptides, such as YAQ₁₂A, can form insoluble β -sheets but, as soluble monomers, have a PPII helical structure. The PPII conformation is also stabilized in polyQ segments by a polyproline segments adjacent to the C-terminal end of the polyQ segment (12, 39).

The foregoing also helps to explain the fact that, in contrast to A β 16–20m and other backbone-modified aggregation inhibitors of β -amyloid and prion peptide aggregation (16, 17, 40, 41), 5QMe₂ did not disassemble preformed fibrils. 5QMe₂ interacts with soluble (PPII-like) YAQ₁₂A, but apparently not with fibrillar (β -sheet) YAQ₁₂A. 5QMe₂ also prevents fibril elongation, possibly by interacting with YAQ₁₂A still in solution. A model of 5QMe₂ action is depicted in Figure 8. According to this model, YAQ₁₂A exists in solution as a PPII-like monomer. It is possible that this peptide can also form oligomers, but we did not observe this, suggesting that oligomers, if present, were present at very low concentrations or were short-lived. Progression to fibril formation requires a transition from PPII to β -sheet conformation, of YAQ₁₂A monomers, oligomers, or both. 5QMe₂ forms transient 1:1 complexes with YAQ₁₂A monomers, thereby maintaining the latter peptide in a PPII-like state. Binding of 5QMe₂ appears to inhibit formation of hydrogen bonds between side chains of YAQ₁₂A molecules. The fact that 5QMe₂ both maintains YAQ₁₂A in a monomeric PPII-like state and also prevents this peptide from forming fibrils suggests that some species with PPII structure may be on-pathway for fibril formation.

Finally, it is appropriate to address the relevance of YAQ₁₂A to aggregation of longer polyQ proteins in biological contexts.

PolyQ peptides and proteins have a sharp threshold for aggregation into fibrils, but this threshold is context-dependent (12, 42, 43). In the context of the protein huntingtin, this threshold is \sim 35 glutamine residues, which is shown by the occurrence of disease in people with CAG triplet expansions of the gene (1), in model systems such as *Caenorhabditis elegans* and *Saccharomyces cerevisiae* (44, 45), and in studies of recombinant htt exon 1-encoded protein in vitro (2, 3). In spinocerebellar ataxia (SCA) type 6, however, the threshold for disease is considerably shorter. The gene for this disease encodes the α 1_A voltage-dependent calcium channel subunit, and disease and intracellular protein aggregates occur when the polyQ expansion exceeds 20–30 residues (43). For peptides without neighboring domains, even as few as six Q residues is sufficient to form β -sheet-rich fibrils (12), and YAQ₁₂A clearly is above this threshold (Figure 7B). Thus, while the threshold might change with context, inhibitors such as 5QMe₂ can serve as structural probes of the aggregation pathway of biologically relevant polyQ peptides and proteins. Finally, although we have used this inhibitor peptide primarily as a structural probe, it could possibly also serve as the basis of an avenue of therapeutic approach.

ACKNOWLEDGMENT

We thank Hélène Auer for assistance with peptide synthesis and purification and Gregory Darnell for helpful discussions. We thank Yimei Chen of the Electron Microscopy Facility, Elena Solomaha of the Biophysics Facility, and Jin Qin at the Chemistry Mass Spectrometry Facility, at the University of Chicago.

SUPPORTING INFORMATION AVAILABLE

A derivation of the equations and other details needed for analysis of equilibrium sedimentation analytical ultracentrifugation of two dissimilar interacting species; determination of \bar{v} for YAQ₁₂A and 5QMe₂; reverse phase HPLC isocratic analysis of YAQ₁₂A remaining in solution, in the presence or absence of 5QMe₂; experiments showing the effect of added fibril seeds on fibrillation of YAQ₁₂A; electron micrograph of a fibril seed slurry used in the preceding experiments; example of analytical ultracentrifugation of YAQ₁₂A and 5QMe₂, showing no improvement of the fit from the addition of higher-order terms in either species; table of comparison of data fits, according to the Akaike Information Criterion, showing improvement of fits by adding a term for a complex between YAQ₁₂A and 5QMe₂; calibration of a Superdex Peptide 10/300 GL column with molecular weight standards; and data showing the absence of a small zone effect in chromatography using the Superdex Peptide column. This material is available free of charge via the Internet at <http://pubs.acs.org>.

REFERENCES

1. The Huntington's Disease Collaborative Research Group (1993) A novel gene containing a trinucleotide repeat that is expanded and unstable on Huntington's disease chromosomes. *Cell* 72, 971–983.
2. Scherzinger, E., Lurz, R., Turmaine, M., Mangiarini, L., Hollenbach, B., Hasenbank, R., Bates, G. P., Davies, S. W., Lehrach, H., and Wanker, E. E. (1997) Huntingtin-encoded polyglutamine expansions form amyloid-like protein aggregates *in vitro* and *in vivo*. *Cell* 90, 549–558.
3. Scherzinger, E., Sittler, A., Schweiger, K., Heiser, V., Lurz, R., Hasenbank, R., Bates, G. P., Lehrach, H., and Wanker, E. E. (1999) Self-assembly of polyglutamine-containing huntingtin fragments into amyloid-like fibrils: Implications for Huntington's disease pathology. *Proc. Natl. Acad. Sci. U.S.A.* 96, 4604–4609.

4. Davies, S. W., Turmaine, M., Cozens, B. A., DiFiglia, M., Sharp, A. H., Ross, C. A., Scherzinger, E., Wanker, E. E., Mangiarini, L., and Bates, G. P. (1997) Formation of neuronal intranuclear inclusions underlies the neurological dysfunction in mice transgenic for the HD mutation. *Cell* 90, 537–548.
5. Chen, S., Berthelie, V., Hamilton, J. B., O'Nuallain, B., and Wetzel, R. (2002) Amyloid-like features of polyglutamine aggregates and their assembly kinetics. *Biochemistry* 41, 7391–7399.
6. Sharma, D., Shinchuk, L. M., Inouye, H., Wetzel, R., and Kirschner, D. A. (2005) Polyglutamine homopolymers having 8–45 residues form slablike β -crystallite assemblies. *Proteins: Struct., Funct., Bioinf.* 61, 398–411.
7. Petkova, A. T., Ishii, Y., Balbach, J. J., Antzutkin, O. N., Leapman, R. D., Delaglio, F., and Tycko, R. (2002) A structural model for Alzheimer's β -amyloid fibrils based on experimental constraints from solid state NMR. *Proc. Natl. Acad. Sci. U.S.A.* 99, 16742–16747.
8. Shewmaker, F., Wickner, R. B., and Tycko, R. (2006) Amyloid of the prion domain of Sup35p has an in-register parallel β -sheet structure. *Proc. Natl. Acad. Sci. U.S.A.* 103, 19754–19759.
9. Wickner, R. B., Dyda, F., and Tycko, R. (2008) Amyloid of Rnq1p, the basis of the [PIN⁺] prion, has a parallel in-register β -sheet structure. *Proc. Natl. Acad. Sci. U.S.A.* 105, 2403–2408.
10. Chimon, S., and Ishii, Y. (2005) Capturing intermediate structures of Alzheimer's β -amyloid, A β (1–40), by solid-state NMR spectroscopy. *J. Am. Chem. Soc.* 127, 13472–13473.
11. Poirier, M. A., Li, H., Macosko, J., Cai, S., Amzel, M., and Ross, C. A. (2002) Huntingtin spheroids and protofibrils as precursors in polyglutamine fibrilization. *J. Biol. Chem.* 277, 41032–41037.
12. Darnell, G., Orgel, J. P. R. O., Pahl, R., and Meredith, S. C. (2007) Flanking polyproline sequences inhibit β -sheet structure in polyglutamine segments by inducing PPII-like helix structure. *J. Mol. Biol.* 374, 688–704.
13. Nagai, Y., Tucker, T., Ren, H., Kenan, D. J., Henderson, B. S., Keene, J. D., Strittmatter, W. J., and Burke, J. R. (2000) Inhibition of polyglutamine protein aggregation and cell death by novel peptides identified by phase display screening. *J. Biol. Chem.* 275, 10437–10442.
14. Nagai, Y., Fujikake, N., Ohno, K., Higashiyama, H., Popiel, H. A., Rahadian, J., Yamaguchi, M., Strittmatter, W. J., Burke, J. R., and Toda, T. (2003) Prevention of polyglutamine oligomerization and neurodegeneration by the peptide inhibitor QBP1 in *Drosophila*. *Hum. Mol. Genet.* 12, 1253–1260.
15. Thakur, A. K., Yang, W., and Wetzel, R. (2004) Inhibition of polyglutamine aggregate cytotoxicity by a structure-based elongation inhibitor. *FASEB J.* 18, 923–925.
16. Gordon, D. J., Sciarretta, K. L., and Meredith, S. C. (2001) Inhibition of β -amyloid(40) fibrillogenesis and disassembly of β -amyloid(40) fibrils by short β -amyloid congeners containing N-methyl amino acids at alternate residues. *Biochemistry* 40, 8237–8245.
17. Gordon, D. J., Tappe, R., and Meredith, S. C. (2002) Design and characterization of a membrane permeable N-methyl amino acid-containing peptide that inhibits A β 1–40 fibrillogenesis. *J. Pept. Res.* 60, 37–55.
18. Darnell, G. D., Derryberry, J. M., Kurutz, J. W., and Meredith, S. C. (2009) Mechanism of Cis-Inhibition of PolyQ Fibrillation by PolyP: PPII Oligomers and the Hydrophobic Effect. *Biophys. J.* 97, 2295–2305.
19. Biron, E., Chatterjee, J., and Kessler, H. (2006) Optimized selective N-methylation of peptides on solid support. *J. Pept. Sci.* 12, 213–219.
20. O'Nuallain, B., Thakur, A. K., Williams, A. D., Bhattacharyya, A. M., Chen, S., Thiagarajan, G., and Wetzel, R. (2006) Kinetics and thermodynamics of amyloid assembly using a high-performance liquid chromatography-based sedimentation assay. *Methods Enzymol.* 413, 34–74.
21. Yamaoka, K., Tanigawara, Y., Nakagawa, T., and Uno, T. (1981) A pharmacokinetic analysis program (MULTI) for microcomputer. *J. Pharm. Dyn.* 4, 879–885.
22. De Mol, N. J., and Fischer, M. J. E. (2008) Kinetic and Thermodynamic Analysis of Ligand–Receptor Interactions: SPR Applications in Drug Development. In *Handbook of Surface Plasmon Resonance* (Schasfoort, R. B. M., and Tudos, A. J., Eds.) 1st ed., pp 123–172, Royal Society of Chemistry, London.
23. Winzor, D. J., Jacobsen, M. P., and Wills, P. R. (1998) Direct Analysis of Sedimentation Equilibrium Distributions Reflecting Complex Formation between Dissimilar Reactants. *Biochemistry* 37, 2226–2233.
24. Milthorpe, B. K., Jeffrey, P. D., and Nichol, L. W. (1975) The direct analysis of sedimentation equilibrium results obtained with polymerizing systems. *Biophys. Chem.* 3, 169–176.
25. Nichol, L. W., Jeffrey, P. D., and Milthorpe, B. K. (1976) The sedimentation equilibrium of heterogeneously associating systems and mixtures of non-interacting solutes: Analysis without determination of molecular weight averages. *Biophys. Chem.* 4, 259–267.
26. Jeffrey, P. D., Nichol, L. W., and Teasdale, R. D. (1979) Studies of macromolecular heterogeneous associations involving cross-linking: A re-examination of the ovalbumin-lysozyme system. *Biophys. Chem.* 10, 379–387.
27. Lebowitz, J., Lewis, M. S., and Schuck, P. (2002) Modern analytical ultracentrifugation in protein science: A tutorial review. *Protein Sci.* 11, 2067–2079.
28. Pallitto, M. M., and Murphy, R. M. (2001) A mathematical model of the kinetics of β -amyloid fibril growth from the denatured state. *Biophys. J.* 81, 1805–1822.
29. Bhattacharyya, A. M., Thakur, A. K., and Wetzel, R. (2005) Polyglutamine aggregation nucleation: Thermodynamics of a highly unfavorable protein folding reaction. *Proc. Natl. Acad. Sci. U.S.A.* 102, 15400–15405.
30. Akaike, H. (1974) A new look at the statistical model identification. *IEEE Trans. Autom. Control* 19, 716–723.
31. Chellgren, B. W., Miller, A. F., and Creamer, T. P. (2006) Evidence for polyproline II helical structure in short polyglutamine tracts. *J. Mol. Biol.* 361, 362–371.
32. Shi, Z., Chen, K., Liu, Z., Sosnick, T. R., and Kallenbach, N. R. (2006) PPII structure in the model peptides for unfolded proteins: Studies on ubiquitin fragments and several alanine-rich peptides containing QQQ, SSS, FFF, and VVV. *Proteins: Struct., Funct., Bioinf.* 63, 312–321.
33. Chellgren, B. W., and Creamer, T. P. (2004) Short sequences of non-proline residues can adopt the polyproline II helical conformation. *Biochemistry* 43, 5864–5869.
34. Shi, Z., Woody, R. W., and Kallenbach, N. R. (2002) Is polyproline II a major backbone conformation in unfolded proteins? *Adv. Protein Chem.* 62, 163–240.
35. Starikov, E. B., Lehrach, H., and Wanker, E. E. (1999) Folding of oligoglutamines: A theoretical approach based on thermodynamics and molecular mechanics. *J. Biomol. Struct. Dyn.* 17, 409–427.
36. Esposito, L., Paladino, A., Pedone, C., and Vitagliano, L. (2008) Insights into structure, stability, and toxicity of monomeric and aggregated polyglutamine models from molecular dynamics simulations. *Biophys. J.* 94, 4031–4040.
37. Miyata, Y., and Yahara, I. (1995) Interaction between Casein Kinase II and the 90-kDa stress protein, HSP90. *Biochemistry* 34, 8123–8129.
38. Maeda, H., Sahara, H., Mori, Y., Torigo, T., Kamiguchi, K., Tamura, Y., Tamura, Y., Hirata, K., and Sato, N. (2007) Biological heterogeneity of the peptide-binding motif of the 70-kDa heat shock protein by surface plasmon resonance analysis. *J. Biol. Chem.* 282, 26956–26962.
39. Bhattacharyya, A., Thakur, A. K., Chellgren, V. M., Thiagarajan, G., Williams, A. D., Chellgren, B. W., Creamer, T. P., and Wetzel, R. (2006) Oligoproline effects on polyglutamine conformation and aggregation. *J. Mol. Biol.* 355, 524–535.
40. Madine, J., Doig, A. J., and Middleton, D. A. (2008) Design of an N-Methylated Peptide Inhibitor of α -Synuclein Aggregation Guided by Solid-State NMR. *J. Am. Chem. Soc.* 130, 7831–7881.
41. Hughes, E., Burke, R. M., and Doig, A. J. (2000) Inhibition of toxicity in the β -amyloid peptide fragment β -(25–35) using N-methylated derivatives: A general strategy to prevent amyloid formation. *J. Biol. Chem.* 275, 25109–25115.
42. Nozaki, K., Onodera, O., Takano, H., and Tsuji, S. (2001) Amino acids flanking polyglutamine stretches influence their potential for aggregate formation. *NeuroReport* 12, 3357–3364.
43. Shizuka, M., Watanabe, M., Ikeda, Y., Mizushima, K., Okamoto, K., and Shoji, M. (1998) Molecular analysis of a de novo mutation for spinocerebellar ataxia type 6 and (CAG)_n repeat units in normal elder controls. *J. Neurol. Sci.* 161, 85–87.
44. Morley, J. F., Brignull, H. R., Weyers, J. J., and Morimoto, R. I. (2002) The threshold for polyglutamine-expansion protein aggregation and cellular toxicity is dynamic and influenced by aging in *Caenorhabditis elegans*. *Proc. Natl. Acad. Sci. U.S.A.* 99, 10417–10422.
45. Krobitsch, S., and Lindquist, S. (2000) Aggregation of huntingtin in yeast varies with the length of the polyglutamine expansion and the expression of chaperone proteins. *Proc. Natl. Acad. Sci. U.S.A.* 97, 1589–1594.